Measurement report: Comparison of wintertime individual particles at ground level and above the mixed layer in urban Beijing

Wenhua Wang[1,2,3], Longyi Shao[1*], Claudio Mazzoleni[3], Yaowei Li[1], Simone Kotthaus[4], Sue Grimmond[4], Janarjan Bhandari[3], Jiaoping Xing[1,5], Xiaolei Feng[1], Mengyuan Zhang[1], Zongbo Shi[6]

1. State Key Laboratory of Coal Resources and Safe Mining & College of Geosciences and Surveying Engineering, China University of Mining and Technology, Beijing, 100083, China
2. School of Resources and Materials, Northeastern University at Qinhuangdao, Qinhuangdao, 066004, China
3. Atmospheric Sciences Program & Physics Department, Michigan Technological University, Houghton, 49931, USA
4. Department of Meteorology, University of Reading, Reading, RG6 6BB, UK
5. School of Forestry, Jiangxi Agricultural University, Nanchang, 330045, China
6. School of Geography Earth and Environmental Sciences, the University of Birmingham, Birmingham, B15 2TT, UK

* Corresponding author: ShaoL@cumtb.edu.cn

Abstract:

Beijing has been suffering from frequent severe air pollution events, with concentrations affected significantly by the mixed layer height. Major efforts have been made to study the physico-chemical properties, compositions, and sources of aerosol particles at ground level. However, little is known about the morphology, elemental composition, and mixing state of aerosol particles above the mixed layer. In this work, we collected individual aerosol particles simultaneously at ground level (2 m above ground) and above the mixed layer in urban Beijing (within the Atmospheric Pollution and Human Health in a Chinese Megacity (APHH-Beijing) 2016 winter campaign). The particles were analyzed off-line by transmission electron microscopy coupled with energy dispersive X-ray spectroscopy. Our results showed that the relative number contribution of mineral particles to all measured particles was much higher during non-haze periods (42.5%) than haze periods (18.1%); on the contrary, internally mixed particles contributed more during haze periods (21.9%) than non-haze periods (7.2%) at ground level. In addition, more mineral particles were found at ground level than above the mixed layer height. Around 20% of individual particles showed core-shell structures during haze periods, whereas only a few core-shell particles were observed during non-haze periods (2%). The results showed that the particles above the mixed layer were more aged with a larger proportion of organic particles originated from coal combustion. Our results indicate that a large fraction of the airborne particles above the mixed layer come from surrounding areas influenced by coal combustion activities. This source contributes to the surface particle concentrations in Beijing when polluted air is mixed down to the ground level.

Keywords: haze; individual particle; organic particle; core-shell structure; mixed layer.

1. Introduction

Atmospheric aerosols emitted from anthropogenic or natural sources are composed of a variety of chemical components (e.g., organic matter, black carbon, nitrate, sulfate, ammonium, metals, mineral dust) (Merikallio et al., 2011; Guo et al., 2014;Wang et al., 2016; Peng et al., 2016; Shao et al., 2017; Tao et al., 2017). Anthropogenic aerosols have received increasing attention in recent decades due to their effects on climate and the environment. In fact, anthropogenic aerosols affect climate through cloud condensation nuclei activity (Kerminen et al., 2012), hygroscopic growth (Brock et al., 2016), and light scattering and absorption (Jacobson, 2001; Bond and Bergstrom, 2006; Merikallio et al., 2011; China et al., 2013; Peng et al., 2016; Bhandari et al., 2019b). They can also have adverse effects on human health, for example, by carrying toxic and carcinogenic compounds (Chen et al., 2013; Shao et al., 2016, 2017). High concentrations of aerosol particles in urban air can cause cardiovascular, respiratory, and even nervous system diseases (Xia et al., 2018; De Marco et al., 2019; Shou et al., 2019). It is suggested that outdoor air pollution causes 3.3 million people premature deaths worldwide each year (Lelieveld et al., 2015). Atmospheric aerosol particles also affect regional and global geochemical cycles as they are transported over long distances (Heald et al., 2006; Weijun Li et al., 2017; Rodriguez-Navarro et al., 2018).

Recently, China has suffered from severe air pollution conditions, like other countries undergoing rapid social and economic development (Huang et al., 2014). In China, urban air pollution is characterized by frequent occurrence of haze events, high $PM_{2.5}$ mass level, and expanded haze areas (Guo et al., 2014; Huang et al., 2014; Sun et al., 2014). For example, the maximum hourly average $PM_{2.5}$ mass concentrations in winter in Beijing reached more than 1000 $\mu g\ m^{-3}$ (Li et al., 2017a; Zhang et al., 2017), 40 times above the safe level of 25 $\mu g\ m^{-3}$ recommended by the World Health Organization (WHO).

As the megacity capital, Beijing has received much attention being one of the most polluted cities in China. Atmospheric researchers have been studying aerosol particles to understand haze formation in China (Sun et al., 2013; Huang et al., 2014; Zhou et al., 2018b). Measurements and model analyses highlight the key roles of secondary aerosol formation by trace gases (e.g., volatile organic compounds, and SO_2, NO_x) and stagnant meteorological conditions in the regional haze formation (Wang et al., 2013; Guo et al., 2014; Huang et al., 2014).

Because the characterization of aerosol particles is mainly focused on surface level observations, the understanding of aerosol properties at higher altitudes in urban areas is still insufficient (Zhou et al., 2018a). Vertical differences between precursors, oxidants and temperature gradients might influence gas-particle partitioning and heterogeneous reactions of N_2O_5 (Zhou et al., 2018a). Previous measurements at the Institute of Atmospheric Physics (IAP) meteorological tower in Beijing showed complex vertical distributions of particulate matter and gaseous pollutants (Meng et al., 2008; Sun et al., 2015; Wang et al., 2018; Zhou et al., 2018b). However, most of these studies focused on non-refractory submicron species. Research showed that the mixed layer height (MLH) could explain some of the vertical difference of aerosol particle chemical composition (Sun et al., 2015; Wang et al., 2018; Zhang et al., 2012). For example, vertical distributions of aerosol particles were more uniform during periods with higher MLH (Wang et al., 2018). As heavily increased air pollution could reduce boundary layer heights by diminishing incoming solar energy and therefore by weakening vertical turbulence, near-surface aerosol concentrations become elevated (Petaja et al., 2016). Moreover, the upper layer particles could influence those below the MLH by downward entrainment or mixing plumes, making the lower layer particles more complex (Wehner et al., 2010; Platis et al., 2015; Qi et al., 2019). Previous studies showed that the particles above the MLH considerably influenced cloud formation (Carnerero et al., 2018) and showed strong aerosol-radiation effect (Bond and Bergstrom, 2006). The differences in aerosol types at ground level and at higher altitudes could lead to large differences in aerosol direct forcing estimates (Ramanathan et al., 2002; Li et al., 2010). The vertical difference of aerosol particles also increases the uncertainties in the assessment of the climate system (Li et al., 2017b). Therefore, a detailed knowledge of the vertical distribution and chemical composition of aerosols is important for understanding the impact on climate and the aerosol evolution process (Zhang et al., 2009; Wang et al., 2018).

Vertical comparisons of individual aerosol particles and their morphologies, mixing states, and elemental compositions are very limited. Transmission Electron Microscopy (TEM) can provide detailed individual particle characterization and help to explain heterogeneous reactions and aging process (Li et al., 2016a). In this study, we compare particles simultaneously collected at ground level and above the MLH based on the meteorological tower at IAP in Beijing, as part of the UK-

CHINA atmospheric pollution and Human Health (APHH) 2016 winter campaign.

2. Experimental

2.1. Aerosol sampling

Individual aerosol samples were collected at the tower division of IAP, Chinese Academy of Science (39°58′N, 116°22′E), in Beijing from 1 to 9 December of 2016. The site, located between the north 3rd and 4th ring roads in Beijing, is influenced by surrounding and regional traffic, and commercial, as well as, residential activities (Sun et al., 2016). There is a highway 250 m East of IAP.

Two DKL-2 single stage cascade impactors, with a 0.5-mm-diameter jet nozzle and a flow rate of 1 L min^{-1} were used. The sampler collection efficiency is ~ 100% at an aerodynamic diameter of 0.5 μm if the particle density is 2 $g \cdot cm^{-3}$ (Li et al., 2016b). Copper (Cu) TEM grids, coated with carbon film (300-mesh; Tianld Co.; Beijing, China), were used to collect the aerosol samples. The sampling duration varied from 30 seconds to less than 5 minutes depending on the air pollution load. Simultaneous observations at ground level (Z1; 2 m above ground) and an elevated altitude (Z2; 280 m above ground) enabled us to obtain the vertical profile of the particles. The collected samples were stored in a dry plastic tube and placed in an air dryer to minimize particle changes before analysis.

Automatic Lidar and Ceilometer (ACL) observations of attenuated backscatter were conducted at the site using a Vaisala CL31 sensor. Measurements were corrected to account for instrument-related background and near range artefacts (Kotthaus et al., 2016). The MLH was derived from profile measurements using the automatic CABAM algorithm (Kotthaus and Grimmond, 2018). Since the TEM samples were collected for less than 5 minutes, the MLH at 15 min resolution was used to determine whether the Z2 observations were located within the MLH or above the MLH (Shi et al., 2019).

Samples were obtained during the periods shown (solid dots and dashed lines) in Fig. 1. Detailed sample information is provided in Table 1. Other measurements including $PM_{2.5}$, SO_2, NO_2, and O_3 mass concentrations at ground level were obtained from the Olympic Park monitor site, which is the closest national air quality monitor station to IAP (~1.5 km) (Shi et al., 2019). City average temperature (T) and relative humidity (RH) at ground level were obtained from the Ministry

of Ecology and Environment of China (https://www.aqistudy.cn/). In this study, the particles were all collected in the morning and midnight when the MLH was the lowest and the height of the tower could reach the MLH at that time.

2.2. Individual particle analysis

Individual particles were analyzed using a JEOL JEM-2800 TEM at an accelerating voltage of 200 kV. The morphology and mixing state of individual particles were determined from the TEM images. Semi-quantitative elemental composition was determined using Energy Dispersive X-ray Spectroscopy (EDS), by which elements heavier than Boron (Z>5) can be detected. Cu was not included because the TEM grids were made of copper. The EDS collection duration of each individual particle was about 15 s to reduce damage of particles from the electron beam. For most particles, only one spectrum of each particle was collected and the spot size of beam would be adjusted according to the size of the particles. Therefore, we obtained the average elemental compositions of each particle. However, more than one spots per particle were collected if the particles were inhomogeneous particles according to the TEM images. The aerosol particles were not evenly distributed on the TEM grids; the coarser particles occurred near the center and the finer particles occurred on the periphery. To ensure a representative data analysis, three or four meshes from the center to the periphery were selected and analyzed. The projected areas of individual particles were determined using the Image-J software (Schneider et al., 2012), which was commonly used for counting and measuring the projected area of atmospheric particles acquired by electron microscopes (Unga et al., 2018). First, the gray-scale images of the particles were converted into binary images, in which black pixels represented the particles and white pixels represented the background. The area equivalent diameters (D_{Aeq}) of the particles are calculated by the following formula: $D_{Aeq} = 2 \cdot (A/\pi)^{1/2}$, where A is the projected area of the particles shown in the TEM images (Bhandari et al., 2019a). Most of the particles with diameter larger than 100 nm were analyzed in this study.

3. Results and discussions

3.1. Mass concentration of air pollutants

The temporal variations of different air pollutants and meteorological conditions at ground level are shown in Fig. 1. The hourly averaged $PM_{2.5}$ mass concentration at the Olympic Park

monitoring site ranged from 3 to 530 μg m^{-3}, with a sample period average of 113.3 μg m^{-3}, significantly exceeding the safe level of 75 μg m^{-3} according to the Chinese National Ambient Air Quality Standard (GB3095-2012). The MLH ranged from 54 to 1496 m, with an average of 397 m. The MLH showed obvious diurnal variation. The hourly mean RH ranged from 17% to 97%, with a 9 day mean of 50.3%. The RH and $PM_{2.5}$ were positively correlated (correlation coefficient=0.75; Fig. S1) according to the 216 groups of hourly data, suggesting that higher RH favors the formation of haze (Sun et al., 2014;Wang et al., 2016). As expected, RH and temperature were negatively correlated (correlation coefficient=-0.51; Fig. S2). The variation trend of SO_2 was similar to that of NO_2. However, the average concentration of NO_2 (83.2 μg m^{-3}) was nearly 5.5 times higher than that of SO_2 (15.2 μg m^{-3}). The concentration of O_3 showed a different trend compared with NO_2 and SO_2 (Fig. 1), with a 9 days hourly mean concentration of 20 μg m^{-3}.

3.2. Classification and mixing state of individual particles

Aerosol particles are classified using their morphologies and elemental compositions into seven main types, namely: 1) organic particles (OPs), 2) sulfur-rich (S-rich) particles, 3) soot particles, 4) mineral particles, 5) metal particles, 6) internally mixed organic and sulfur-rich particles (OP-S), and 7) other mixed particles. The detailed characteristics of each particle type are shown in Table 2.

OPs are mainly composed of C and O, usually with a small amount of Si, S, Cl, and K. OPs are relatively stable under the electron beam irradiation. Based on the morphologies, OPs can be further divided into spherical (Fig. 2a) and irregularly shapes (Fig. 2b). They are mainly from combustion process of biomass and fossil fuel (Li et al., 2016a).

S-rich particles (Figs. 2c and 2d) are mainly composed of O, S, and N, and sometimes also contain some amount of K. S-rich particles are beam-sensitive and volatilize under strong beam irradiation. S-rich particles generally represent secondary inorganic components (e.g., SO_4^{2+}, NO_3^- and NH_4^+) (Xu et al., 2019).

Soot particles are mainly composed of C, minor amount of O, and sometimes Si. Soot particles consist of a number of C-dominated spherical monomers less than 100 nm in diameter (Figs. 2e and 2f) and can be easily identified under high-resolution TEM (Buseck et al., 2014; Bhandari et al., 2017). Soot particles, stable under the electron beam, show chain-like or compact morphologies in

the atmosphere (Sorensen et al., 2001; Adachi et al., 2007; China et al., 2013, 2015; Bhandari et al., 2019a). Soot particles are mainly from incomplete combustion of biomass and fossil fuel.

Metal particles (Figs. 2g and 2h) and mineral particles (Fig. 2i) are stable under the beam irradiation. Mineral particles are mostly irregularly shaped containing crustal elements (e.g., Si, Al, Ca, Fe, Na, K, Mg, Ti, and S) in addition to O. They can be generated from windblown soil dust or road dust. Metal particles are spherical or near spherical and are mainly composed of Fe, Zn, Mn, Ti, and Pb. Metal particles ae mainly originated from industries, coal-fired power plants, and oil refineries (Xu et al., 2019) or vehicle brakes (Hou et al., 2018).

Internally mixed particles (Figs. 2j-p) are particles with at least two of the above components. They usually show relative larger diameter. We further classify them as internally mixed organic and sulfur-rich particles (OP-S) (Figs. 2j-l), and other mixed particles (Figs. 2m-p).

3.3. Comparison of haze and non-haze individual particle at ground level

Haze periods are defined as hourly average $PM_{2.5}$ mass concentration greater than 75 μg m^{-3} during collection time; the rest are defined as non-haze periods. A total of 1538 individual particles among 8 samples at ground level were analyzed based on the TEM results. The relative number percentage (N(type i)/ N(total)*100) of particles in each sample was calculated. The results are provided in Table 3 and shown in Fig.3. During non-haze periods, the particles were composed of mineral particles (42.5%), OPs (21.1%), S-rich particles (20.0%), soot particles (6.4%), other mixed particles (5.6%), metal particles (2.83%), and OP-S (1.6%) in descending order. During haze periods, the particles were composed of OPs (28.3%), S-rich particles (23.5%), mineral particles (18.1%), OP-S (13.1%), other mixed particles (8.8%), soot particles (6.6%), and metal particles (1.7%) in descending order.

The mineral particles are mainly from re-suspended road dust, soil dust, and construction dust during non-desert transport dust episodes (Sun et al., 2006; Gao et al., 2016; Wang et al., 2017). The relative number percentage of mineral particles was much higher during non-haze periods (42.5%) than during haze periods (18.1%), as shown in Fig.3.

However, the content of mixed particles including OP-S and other mixed particles during haze periods (21.9%) was much higher than during non-haze periods (7.2%), suggesting that there was more secondary aerosol formation during haze periods. High secondary aerosol formation in winter

in Beijing during the pollution periods was also found in previous studies (Huang et al., 2014; Sun et al., 2016; Li et al., 2017a). Secondary aerosol formation was expected since the RH during the haze periods were relatively higher than during non-haze periods, as shown in Table 1 and Fig.1, which facilitated chemical reactions of gaseous pollutants (Liu et al., 2016; Wang et al., 2016). Also, the average content of OPs and S-rich were higher during haze periods than during non-haze periods.

3.4. Comparison of individual particles at ground level and above the MLH

A total of 1519 individual particles among 8 samples above the MLH were analyzed. The results are provided in Table 3 and shown in Fig. 3. We found that the relative number percentage of mineral particles at ground level was larger than that above the MLH. For example, mineral particles at ground level and above the MLH during non-haze periods accounted for 42.5% and 23.2%, respectively, and during haze periods the values are 18.1% and 9.5%, respectively. S-rich particles during non-haze periods accounted for 20.0% at ground level, less than the value of 30.7% above the MLH. However, not all the samples above the MLH during haze periods showed higher relative number percentage of S-rich particles than at ground level. This might because some of the S-rich particles above the MLH were mixed with other particles, forming mixed particles. Another reason might be that higher relative number percentage of mixed particles diluted the relative number percentage of S-rich particles. The mixed particles during haze periods accounted for 32.0% above the MLH, higher than that of 21.9% at ground level. We also found that OPs above the MLH accounted for higher relative number percentage than at ground level, although there was some variance. For example, samples 4 and 6 showed higher relative number percentage of OPs at ground level. That might because that some of the OPs were mixed with S-rich particles and OP-S showed higher relative number percentage above the MLH than at ground level in samples 4 and 6. Metals and soot only accounted for a few relative number percentages in all samples and they didn't show much difference at ground level and above the MLH. Particles above the MLH were either transported from the surrounding areas or from ground sources. In both cases, they were subject to atmospheric process, leading to their aging.

3.5. Aging of particles

In the atmosphere, particles are subjected to aging process. During the aging process of aerosol particles, secondary species can coat pre-existing particles (Li and Shao, 2009; Laskin et al., 2016;

Li et al., 2016b; Niu et al., 2016; Tang et al., 2016; Chen et al., 2017; Hou et al., 2018; Unga et al., 2018; Xu et al., 2019). Using high-resolution TEM images, it is possible to identify the core-shell structure of particles (Li et al., 2016a). For example, Figs. 4a and 4b showed S-rich particles coated by secondary species. Figs. 4c and 4d were OPs coated with secondary species. Figs. 4e-h showed core-shell structured particles with some mixed particle cores. In this study, we found that the core-shell structured particles accounted for 20% during haze periods with 17% at ground level and 23% above the MLH, but only 2% during non-haze periods. These results demonstrated a general trend that the core-shell structured particles during haze periods were much higher than during non-haze periods. Also, the average D_{Aeq} of particles was larger during haze periods than during non-haze periods as shown in Fig. S3. These results confirmed that particles during haze periods underwent more extensive aging than during non-haze periods.

The coating of atmospheric particles is often caused by aging mechanisms such as coagulation, condensation, and heterogeneous chemical reactions (Kahnert, 2015; Müller et al., 2017, Zhang et at., 2012). Fig. 5 shows low magnification images of particles at ground level and above the MLH. More core-shell particles were found above the MLH. The core/shell ratio (R), which is the ratio of the D_{Aeq} of core to the D_{Aeq} of whole particle including the coating, has been used to evaluate the aging process of aerosol particles in different studies (Niu et al., 2012, 2016; Hou et al., 2018). The value of R ranged from 0 to less than 1. A smaller R value means the particles are more coated, thus are subjected to a more extensive degree of aging (Hou et al., 2018). Because high number percentage of core-shell structured particles were only found during haze periods, we only measured R of core-shell structured particles during the haze periods (including the samples 2, 4, 5, 6 and 7). Fig. 6a shows the R value of each samples during the haze periods. We can see from Fig. 6a that all the samples showed a smaller average R value above the MLH compared with those from the ground level. The average R value above the MLH (0.54) was smaller than ground level (0.59). Additionally, the relative number percentage of core-shell structured particles was higher above the MLH than at ground level, except for sample 4. These findings indicated that the particles above the MLH were more aged than those at ground level.

Fig. S3 shows the total particle number-size distribution; the relative number percentage of the larger size particles clearly increased when considering the coatings compared to only considering

the core size during haze periods. The change in optical properties due to coating was calculated in various studies by using different methods (Cappa et al., 2012; Scarnato et al., 2013; Liu et al., 2015; Saliba et al., 2016; Unga et al., 2018). When host particles were coated, their optical properties might be amplified (Khalizov et al., 2009; Peng et al., 2016). Also, organic coating can influence the hygroscopic properties and the viscosity of mixed particles (Sharma et al., 2018; Unga et al., 2018), and thus can influence cloud formation activity (Kerminen et al., 2012).

3.6. Possible sources of organic particles

Our results showed higher relative number percentage of OPs both during non-haze (21.1%) and haze periods (28.3%) in winter Beijing, compared with a tunnel environment (~5%), where the vehicle emissions were the main pollution sources (Hou et al., 2018). Also, recent studies did not find abundant OPs in North China during Spring and Summer (Yuan et al., 2015; Li et al., 2016b; Xu et al., 2019;). Instead, a larger number percentage of OPs have been found in winter using electron microscopy in previous studies, including an outflow of a haze plume in East Asia (Zhu et al., 2013), a coal-burning region in China's Loess Plateau (Li et al., 2012), three sampling sites in North China Plain (Chen et al., 2017) and urban and rural sites in Northeast China (Xu et al., 2017; Zhang et al., 2017). These results suggested that OPs accounted for a large number percentage of the particles in north China in winter.

Most of the OPs in our study were spherical or nearly spherical in shape according to the projected images and they were stable under strong electron beam irradiation and appear dark features in TEM images, which reflected their high thickness and refractory properties (Ebert et al., 2016), suggesting that they were formed through cooling process after the biomass or fossil fuel combustion pyrolysis products of volatile organic compounds were emitted into the atmosphere (Wang et al., 2015; Chen et al., 2017; Zhang et al., 2017).

These spherical or near spherical OPs are considered to be brown carbon (Zhang et al., 2020). Brown carbon plays a significant role in atmospheric shortwave absorption and can cause warming of the atmosphere (Adachi and Buseck, 2011;Hoffer et al., 2016). Some researchers have found that the primary OPs from coal combustion have more Si than those from biomass burning (Li et al., 2012; Chen et al., 2017). The weight ratio of C-O-Si at ground level and above the MLH is shown in Fig. 7. More coal burning related OPs were found above the MLH. Since the relative number

295 percentage of primary OPs affected by coal burning are higher above the MLH than at ground level,
296 OPs above the MLH are not all from ground level and might be originated from surrounding areas
297 influenced by coal combustion. The results were supported by the 24-h backward trajectories, which
298 showed that air masses above the MLH during haze periods were from the North and West direction
299 of Beijing as shown in Fig. S4. It is reasonable that Beijing has implemented strict air pollution
300 controls measures, including using natural gas to replace domestic coal burning. The particles above
301 the MLH can contribute to Beijing air pollution by mixing down to the ground.

302 ## 4. Conclusions

303 Detailed morphologies and elemental compositions of individual aerosol particles at ground level
304 and above the mixed layer height were analyzed in this study. Following conclusions were achieved:

305 1) Particles were classified into organic particles, S-rich particles, mineral particles, metal
306 particles, soot, internally mixed organic and sulfur-rich particles, and other mixed particles.
307 Compared with non-haze periods, haze periods were associated with a relative lower number
308 percentage of mineral particles and a relative higher number percentage of mixed particles.

309 2) Compared with the aerosol samples at ground level, the samples above MLH had a lower
310 relative number percentage of mineral particles, a higher number percentage of coated particles, a
311 smaller core/shell ratio of coated particles. More coated particles and higher core/shell ratio in the
312 aerosol samples above the mixed layer suggested that the particles above the mixed layer were more
313 aged.

314 3) Relative number percentage of organic particles accounted for 21.1% during non-haze periods
315 and 28.3% during haze periods in winter Beijing. More organic particles above the mixed layer were
316 associated with coal combustion according to the C-O-Si ratio, and the long-range transportation of
317 air masses from surrounding areas has an important influence for Beijing air.

318 **Data availability:** Data used in this study are available from the corresponding author upon request
319 (ShaoL@cumtb.edu.cn)

320 **Author Contributions:** WW, LS, CM, JX and ZS conceived the manuscript. WW, WL, XF and
321 MZ conducted the sample collection and analysis. SK and SG conducted the MLH measurement.
322 CM and BJ conducted manuscript modification.

323 **Competing interest:** The authors declare no conflict of interest.

Acknowledgements: We thank Zifa Wang and Pingqing Fu at IAP for the supporting of sample collection. This work was supported by National Natural Science Foundation of China (No. 42075107), International Cooperation Projects of National Natural Science Foundation of China (No. 41571130031), China Scholarship Council (No. 201806430015), Yue Qi Scholar Fund of China University of Mining and Technology (Beijing). CM and JB were supported by the U.S Department of Energy (DOE), Office of Biological and Environmental Research (OBER), Atmospheric System Research (#DE-SC0011935 and Grant # DE-SC0018931). ZS was supported by Natural Environmental Research Council (NE/N007190/1).

Reference:

Adachi, K., Chung, S. H., Friedrich, H., and Buseck, P. R.: Fractal parameters of individual soot particles determined using electron tomography: Implications for optical properties, Journal of Geophysical Research, 112, 10.1029/2006jd008296, 2007.

Adachi, K., and Buseck, P. R.: Atmospheric tar balls from biomass burning in Mexico, J. Geophys. Res.-Atmos., 116, 7, 10.1029/2010jd015102, 2011.

Bhandari, J., China, S., Onasch, T., Wolff, L., Lambe, A., Davidovits, P., Cross, E., Ahern, A., Olfert, J., Dubey, M., and Mazzoleni, C.: Effect of Thermodenuding on the Structure of Nascent Flame Soot Aggregates, Atmosphere, 8, 10.3390/atmos8090166, 2017.

Bhandari, J., China, S., Chandrakar, K. K., Kinney, G., Cantrell, W., Shaw, R. A., Mazzoleni, L. R., Girotto, G., Sharma, N., Gorkowski, K., Gilardoni, S., Decesari, S., Facchini, M. C., Zanca, N., Pavese, G., Esposito, F., Dubey, M. K., Aiken, A. C., Chakrabarty, R. K., Moosmuller, H., Onasch, T. B., Zaveri, R. A., Scarnato, B. V., Fialho, P., and Mazzoleni, C.: Extensive Soot Compaction by Cloud Processing from Laboratory and Field Observations, Sci Rep, 9, 11824, 10.1038/s41598-019-48143-y, 2019a.

Bhandari, J., China, S., Girotto, G., Scarnato, B. V., Gorkowski, K., Aiken, A. C., Dubey, M. K., and Mazzoleni, C.: Optical properties and radiative forcing of fractal-like tar ball aggregates from biomass burning, Journal of Quantitative Spectroscopy and Radiative Transfer, 230, 65-74, 10.1016/j.jqsrt.2019.01.032, 2019b.

Bond, T. C., and Bergstrom, R. W.: Light Absorption by Carbonaceous Particles: An Investigative Review, Aerosol Science and Technology, 40, 27-67, 10.1080/02786820500421521, 2006.

Brock, C. A., Wagner, N. L., Anderson, B. E., Attwood, A. R., Beyersdorf, A., Campuzano-Jost, P., Carlton, A. G., Day, D. A., Diskin, G. S., Gordon, T. D., Jimenez, J. L., Lack, D. A., Liao, J., Markovic, M. Z., Middlebrook, A. M., Ng, N. L., Perring, A. E., Richardson, M. S., Schwarz, J. P., Washenfelder, R. A., Welti, A., Xu, L., Ziemba, L. D., and Murphy, D. M.: Aerosol optical properties in the southeastern United States in summer – Part 1: Hygroscopic growth, Atmospheric Chemistry and Physics, 16, 4987-5007, 10.5194/acp-16-4987-2016, 2016.

Buseck, P. R., Adachi, K., Gelencsér, A., Tompa, É., and Pósfai, M.: Ns-Soot: A Material-Based Term for Strongly Light-Absorbing Carbonaceous Particles, Aerosol Science and Technology, 48, 777-788, 10.1080/02786826.2014.919374, 2014.

Cappa, C. D., Onasch, T. B., Massoli, P., Worsnop, D. R., Bates, T. S., Cross, E. S., Davidovits, P., Hakala, J., Hayden, K. L., Jobson, B. T., Kolesar, K. R., Lack, D. A., Lerner, B. M., Li, S.-M., Mellon, D., Nuaaman, I., Olfert, J. S., Petäjä, T., Quinn, P. K., Song, C., Subramanian, R., Williams, E. J., and Zaveri, R. A.: Radiative Absorption Enhancements Due to the Mixing State of Atmospheric Black Carbon, Science, 337, 1078, 10.1126/science.1223447, 2012.

Carnerero, C., Pérez, N., Reche, C., Ealo, M., Titos, G., Lee, H.-K., Eun, H.-R., Park, Y.-H., Dada, L., Paasonen, P., Kerminen, V.-M., Mantilla, E., Escudero, M., Gómez-Moreno, F. J., Alonso-Blanco, E., Coz, E., Saiz-Lopez, A., Temime-Roussel, B., Marchand, N., Beddows, D. C. S., Harrison, R. M., Petäjä, T., Kulmala, M., Ahn, K.-H., Alastuey, A., and Querol, X.: Vertical and horizontal distribution of regional new particle formation events in Madrid, Atmospheric Chemistry and Physics, 18, 16601-16618, 10.5194/acp-18-

16601-2018, 2018.

Chen, S., Xu, L., Zhang, Y., Chen, B., Wang, X., Zhang, X., Zheng, M., Chen, J., Wang, W., Sun, Y., Fu, P., Wang, Z., and Li, W.: Direct observations of organic aerosols in common wintertime hazes in North China: insights into direct emissions from Chinese residential stoves, Atmospheric Chemistry and Physics, 17, 1259-1270, 10.5194/acp-17-1259-2017, 2017.

Chen, Y., Ebenstein, A., Greenstone, M., and Li, H.: Evidence on the impact of sustained exposure to air pollution on life expectancy from China's Huai River policy, Proc Natl Acad Sci U S A, 110, 12936-12941, 10.1073/pnas.1300018110, 2013.

China, S., Mazzoleni, C., Gorkowski, K., Aiken, A. C., and Dubey, M. K.: Morphology and mixing state of individual freshly emitted wildfire carbonaceous particles, Nat Commun, 4, 2122, 10.1038/ncomms3122, 2013.

China, S., Mazzoleni, C., Gorkowski, K., Aiken, A.C. and Dubey, M.K., 2013. Morphology and mixing state of individual freshly emitted wildfire carbonaceous particles. Nat Commun, 4: 2122.

China, S., Scarnato, B., Owen, R. C., Zhang, B., Ampadu, M. T., Kumar, S., Dzepina, K., Dziobak, M. P., Fialho, P., Perlinger, J. A., Hueber, J., Helmig, D., Mazzoleni, L. R., and Mazzoleni, C.: Morphology and mixing state of aged soot particles at a remote marine free troposphere site: Implications for optical properties, Geophysical Research Letters, 42, 1243-1250, 10.1002/2014gl062404, 2015.

De Marco, A., Proietti, C., Anav, A., Ciancarella, L., D'Elia, I., Fares, S., Fornasier, M. F., Fusaro, L., Gualtieri, M., Manes, F., Marchetto, A., Mircea, M., Paoletti, E., Piersanti, A., Rogora, M., Salvati, L., Salvatori, E., Screpanti, A., Vialetto, G., Vitale, M., and Leonardi, C.: Impacts of air pollution on human and ecosystem health, and implications for the National Emission Ceilings Directive: Insights from Italy, Environ Int, 125, 320-333, 10.1016/j.envint.2019.01.064, 2019.

Ebert, M., Weigel, R., Kandler, K., Günther, G., Molleker, S., Grooß, J. U., Vogel, B., Weinbruch, S., and Borrmann, S.: Chemical analysis of refractory stratospheric aerosol particles collected within the arctic vortex and inside polar stratospheric clouds, Atmos. Chem. Phys., 16, 8405-8421,502 10.5194/acp-16-8405-2016, 2016.

Gao, J., Peng, X., Chen, G., Xu, J., Shi, G. L., Zhang, Y. C., and Feng, Y. C.: Insights into the chemical characterization and sources of PM(2.5) in Beijing at a 1-h time resolution, Sci Total Environ, 542, 162-171, 10.1016/j.scitotenv.2015.10.082, 2016.

Guo, S., Hu, M., Zamora, M. L., Peng, J., Shang, D., Zheng, J., Du, Z., Wu, Z., Shao, M., Zeng, L., Molina, M. J., and Zhang, R.: Elucidating severe urban haze formation in China, Proc Natl Acad Sci U S A, 111, 17373-17378, 10.1073/pnas.1419604111, 2014.

Heald, C. L., Jacob, D. J., Park, R. J., Alexander, B., Fairlie, T. D., Yantosca, R. M., and Chu, D. A.: Transpacific transport of Asian anthropogenic aerosols and its impact on surface air quality in the United States, Journal of Geophysical Research, 111, 10.1029/2005jd006847, 2006.

Hoffer, A., Toth, A., Nyiro-Kosa, I., Posfai, M., and Gelencser, A.: Light absorption properties of laboratory-generated tar ball particles, Atmospheric Chemistry and Physics, 16, 239-246, 10.5194/acp-16-239-2016, 2016.

Hou, C., Shao, L., Hu, W., Zhang, D., Zhao, C., Xing, J., Huang, X., and Hu, M.: Characteristics and aging of traffic-derived particles in a highway tunnel at a coastal city in southern China, Sci Total Environ, 619-620, 1385-1393, 10.1016/j.scitotenv.2017.11.165, 2018.

Huang, R. J., Zhang, Y., Bozzetti, C., Ho, K. F., Cao, J. J., Han, Y., Daellenbach, K. R., Slowik, J. G., Platt, S. M., Canonaco, F., Zotter, P., Wolf, R., Pieber, S. M., Bruns, E. A., Crippa, M., Ciarelli, G., Piazzalunga, A., Schwikowski, M., Abbaszade, G., Schnelle-Kreis, J., Zimmermann, R., An, Z., Szidat, S., Baltensperger, U., El Haddad, I., and Prevot, A. S.: High secondary aerosol contribution to particulate pollution during haze events in China, Nature, 514, 218-222, 10.1038/nature13774, 2014.

Jacobson, M. Z.: Strong radiative heating due to the mixing state of black carbon in atmospheric aerosols, Nature, 409, 695-697, 10.1038/35055518, 2001.

Kahnert, M.: Modelling radiometric properties of inhomogeneous mineral dust particles: Applicability and limitations of effective medium theories, Journal of Quantitative Spectroscopy and Radiative Transfer, 152, 16-27, 10.1016/j.jqsrt.2014.10.025, 2015.

Kerminen, V. M., Paramonov, M., Anttila, T., Riipinen, I., Fountoukis, C., Korhonen, H., Asmi, E., Laakso, L., Lihavainen, H., Swietlicki, E., Svenningsson, B., Asmi, A., Pandis, S. N., Kulmala, M., and Petäjä, T.: Cloud condensation nuclei production associated with atmospheric nucleation: a synthesis based on existing literature and new results, Atmospheric Chemistry and Physics, 12, 12037-12059, 10.5194/acp-12-12037-2012, 2012.

Khalizov, A. F., Xue, H., Wang, L., Zheng, J., and Zhang, R.: Enhanced Light Absorption and Scattering by Carbon Soot Aerosol Internally Mixed with Sulfuric Acid, The Journal of Physical Chemistry A, 113, 1066-1074, 10.1021/jp807531n, 2009.

Kotthaus, S., O'Connor, E., Münkel, C., Charlton-Perez, C., Haeffelin, M., Gabey, A. M., and Grimmond, C. S. B.: Recommendations for processing atmospheric attenuated backscatter profiles from Vaisala CL31 ceilometers, Atmos. Meas. Tech., 9, 3769-3791, 10.5194/amt-9-3769-2016, 2016.

Kotthaus, S., and Grimmond, C. S. B.: Atmospheric boundary-layer characteristics from ceilometer measurements. Part 1: A new method to track mixed layer height and classify clouds, Quarterly Journal of the Royal Meteorological Society, 144, 1525-1538, 10.1002/qj.3299, 2018.

Laskin, A., Gilles, M. K., Knopf, D. A., Wang, B., and China, S.: Progress in the Analysis of Complex Atmospheric Particles, Annu Rev Anal Chem (Palo Alto Calif), 9, 117-143, 10.1146/annurev-anchem-071015-041521, 2016.

Lelieveld, J., Evans, J. S., Fnais, M., Giannadaki, D., and Pozzer, A.: The contribution of outdoor air pollution sources to premature mortality on a global scale, Nature, 525, 367-371, 10.1038/nature15371, 2015.

Li, J., Du, H., Wang, Z., Sun, Y., Yang, W., Li, J., Tang, X., and Fu, P.: Rapid formation of a severe regional winter haze episode over a mega-city cluster on the North China Plain, Environ Pollut, 223, 605-615, 10.1016/j.envpol.2017.01.063, 2017a.

Li, W., and Shao, L.: Transmission electron microscopy study of aerosol particles from the brown hazes in northern China, Journal of Geophysical Research, 114, 10.1029/2008jd011285, 2009.

Li, W., Shi, Z., Zhang, D., Zhang, X., Li, P., Feng, Q., Yuan, Q., and Wang, W.: Haze particles over a coal-burning region in the China Loess Plateau in winter: Three flight missions in December 2010, Journal of Geophysical Research: Atmospheres, 117, n/a-n/a, 10.1029/2012jd017720, 2012.

Li, W., Shao, L., Zhang, D., Ro, C.-U., Hu, M., Bi, X., Geng, H., Matsuki, A., Niu, H., and Chen, J.: A review of single aerosol particle studies in the atmosphere of East Asia: morphology, mixing state, source, and heterogeneous reactions, Journal of Cleaner Production, 112, 1330-1349, 10.1016/j.jclepro.2015.04.050, 2016a.

Li, W., Sun, J., Xu, L., Shi, Z., Riemer, N., Sun, Y., Fu, P., Zhang, J., Lin, Y., Wang, X., Shao, L., Chen, J., Zhang, X., Wang, Z., and Wang, W.: A conceptual framework for mixing structures in individual aerosol particles, Journal of Geophysical Research: Atmospheres, 121, 13,784-713,798, 10.1002/2016jd025252, 2016b.

Li, Z., Lee, K.-H., Wang, Y., Xin, J., and Hao, W.-M.: First observation-based estimates of cloud-free aerosol radiative forcing across China, 115, 10.1029/2009jd013306, 2010.

Li, Z., Guo, J., Ding, A., Liao, H., Liu, J., Sun, Y., Wang, T., Xue, H., Zhang, H., and Zhu, B.: Aerosol and boundary-layer interactions and impact on air quality, National Science Review, 4, 810-833, 10.1093/nsr/nwx117, 2017b.

Liu, S., Aiken, A. C., Gorkowski, K., Dubey, M. K., Cappa, C. D., Williams, L. R., Herndon, S. C., Massoli, P., Fortner, E. C., Chhabra, P. S., Brooks, W. A., Onasch, T. B., Jayne, J. T., Worsnop, D. R., China, S., Sharma, N., Mazzoleni, C., Xu, L., Ng, N. L., Liu, D., Allan, J. D., Lee, J. D., Fleming, Z. L., Mohr, C., Zotter, P., Szidat, S., and Prévôt, A. S. H.: Enhanced light absorption by mixed source black and brown carbon particles in UK winter, Nature Communications, 6, 8435, 10.1038/ncomms9435

https://www.nature.com/articles/ncomms9435#supplementary-information, 2015.

Liu, Z., Hu, B., Zhang, J., Yu, Y., and Wang, Y.: Characteristics of aerosol size distributions and chemical compositions during wintertime pollution episodes in Beijing, Atmospheric Research, 168, 1-12, 10.1016/j.atmosres.2015.08.013, 2016.

Meng, Z. Y., Ding, G. A., Xu, X. B., Xu, X. D., Yu, H. Q., and Wang, S. F.: Vertical distributions of SO(2) and NO(2) in the lower atmosphere in Beijing urban areas, China, Sci Total Environ, 390, 456-465, 10.1016/j.scitotenv.2007.10.012, 2008.

Merikallio, S., Lindqvist, H., Nousiainen, T., and Kahnert, M.: Modelling light scattering by mineral dust using spheroids: assessment of applicability, Atmospheric Chemistry and Physics, 11, 5347-5363, 10.5194/acp-11-5347-2011, 2011.

Müller, A., Miyazaki, Y., Aggarwal, S. G., Kitamori, Y., Boreddy, S. K. R., and Kawamura, K.: Effects of chemical composition and mixing state on size-resolved hygroscopicity and cloud condensation nuclei activity of submicron aerosols at a suburban site in northern Japan in summer, Journal of Geophysical Research: Atmospheres, 122, 9301-9318, 10.1002/2017jd027286, 2017.

Niu, H., Shao, L., and Zhang, D.: Soot particles at an elevated site in eastern China during the passage of a strong cyclone, Sci Total Environ, 430, 217-222, 10.1016/j.scitotenv.2012.04.050, 2012.

Niu, H., Hu, W., Zhang, D., Wu, Z., Guo, S., Pian, W., Cheng, W., and Hu, M.: Variations of fine particle physiochemical properties during a heavy haze episode in the winter of Beijing, Sci Total Environ, 571,

103-109, 10.1016/j.scitotenv.2016.07.147, 2016.

Peng, J., Hu, M., Guo, S., Du, Z., Zheng, J., Shang, D., Levy Zamora, M., Zeng, L., Shao, M., Wu, Y. S., Zheng, J., Wang, Y., Glen, C. R., Collins, D. R., Molina, M. J., and Zhang, R.: Markedly enhanced absorption and direct radiative forcing of black carbon under polluted urban environments, Proc Natl Acad Sci U S A, 113, 4266-4271, 10.1073/pnas.1602310113, 2016.

Petaja, T., Jarvi, L., Kerminen, V. M., Ding, A. J., Sun, J. N., Nie, W., Kujansuu, J., Virkkula, A., Yang, X. Q., Fu, C. B., Zilitinkevich, S., and Kulmala, M.: Enhanced air pollution via aerosol-boundary layer feedback in China, Sci Rep, 6, 18998, 10.1038/srep18998, 2016.

Platis, A., Altstädter, B., Wehner, B., Wildmann, N., Lampert, A., Hermann, M., Birmili, W., and Bange, J.: An Observational Case Study on the Influence of Atmospheric Boundary-Layer Dynamics on New Particle Formation, Boundary-Layer Meteorology, 158, 67-92, 10.1007/s10546-015-0084-y, 2015.

Qi, X., Ding, A., Nie, W., Chi, X., Huang, X., Xu, Z., Wang, T., Wang, Z., Wang, J., Sun, P., Zhang, Q., Huo, J., Wang, D., Bian, Q., Zhou, L., Zhang, Q., Ning, Z., Fei, D., Xiu, G., and Fu, Q.: Direct measurement of new particle formation based on tethered airship around the top of the planetary boundary layer in eastern China, Atmospheric Environment, 209, 92-101, 10.1016/j.atmosenv.2019.04.024, 2019.

Ramanathan, V., Crutzen, P. J., Mitra, A. P., and Sikka, D.: The Indian Ocean Experiment and the Asian Brown Cloud, Curr. Sci., 83, 947-955, 2002.

Rodriguez-Navarro, C., di Lorenzo, F., and Elert, K.: Mineralogy and physicochemical features of Saharan dust wet deposited in the Iberian Peninsula during an extreme red rain event, Atmospheric Chemistry and Physics, 18, 10089-10122, 10.5194/acp-18-10089-2018, 2018.

Saliba, G., Subramanian, R., Saleh, R., Ahern, A. T., Lipsky, E. M., Tasoglou, A., Sullivan, R. C., Bhandari, J., Mazzoleni, C., and Robinson, A. L.: Optical properties of black carbon in cookstove emissions coated with secondary organic aerosols: Measurements and modeling, Aerosol Science and Technology, 50, 1264-1276, 10.1080/02786826.2016.1225947, 2016.

Scarnato, B. V., Vahidinia, S., Richard, D. T., and Kirchstetter, T. W.: Effects of internal mixing and aggregate morphology on optical properties of black carbon using a discrete dipole approximation model, Atmospheric Chemistry and Physics, 13, 5089-5101, 10.5194/acp-13-5089-2013, 2013.

Schneider, C. A., Rasband, W. S., and Eliceiri, K. W.: NIH Image to ImageJ: 25 years of image analysis, Nature Methods, 9, 671-675, 10.1038/nmeth.2089, 2012.

Shao, L., Hou, C., Geng, C., Liu, J., Hu, Y., Wang, J., Jones, T., Zhao, C., and BéruBé, K.: The oxidative potential of PM 10 from coal, briquettes and wood charcoal burnt in an experimental domestic stove, Atmospheric Environment, 127, 372-381, 10.1016/j.atmosenv.2015.12.007, 2016.

Shao, L., Hu, Y., Shen, R., Schafer, K., Wang, J., Wang, J., Schnelle-Kreis, J., Zimmermann, R., BeruBe, K., and Suppan, P.: Seasonal variation of particle-induced oxidative potential of airborne particulate matter in Beijing, Sci Total Environ, 579, 1152-1160, 10.1016/j.scitotenv.2016.11.094, 2017.

Sharma, N., China, S., Bhandari, J., Gorkowski, K., Dubey, M., Zaveri, R. A., and Mazzoleni, C.: Physical Properties of Aerosol Internally Mixed With Soot Particles in a Biogenically Dominated Environment in California, Geophysical Research Letters, 45, 11,473-411,482, 10.1029/2018gl079404, 2018.

Shi, Z., Vu, T., Kotthaus, S., Harrison, R. M., Grimmond, S., Yue, S., Zhu, T., Lee, J., Han, Y., Demuzere, M., Dunmore, R. E., Ren, L., Liu, D., Wang, Y., Wild, O., Allan, J., Acton, W. J., Barlow, J., Barratt, B., Beddows, D., Bloss, W. J., Calzolai, G., Carruthers, D., Carslaw, D. C., Chan, Q., Chatzidiakou, L., Chen, Y., Crilley, L., Coe, H., Dai, T., Doherty, R., Duan, F., Fu, P., Ge, B., Ge, M., Guan, D., Hamilton, J. F., He, K., Heal, M., Heard, D., Hewitt, C. N., Hollaway, M., Hu, M., Ji, D., Jiang, X., Jones, R., Kalberer, M., Kelly, F. J., Kramer, L., Langford, B., Lin, C., Lewis, A. C., Li, J., Li, W., Liu, H., Liu, J., Loh, M., Lu, K., Lucarelli, F., Mann, G., McFiggans, G., Miller, M. R., Mills, G., Monk, P., Nemitz, E., amp, apos, Connor, F., Ouyang, B., Palmer, P. I., Percival, C., Popoola, O., Reeves, C., Rickard, A. R., Shao, L., Shi, G., Spracklen, D., Stevenson, D., Sun, Y., Sun, Z., Tao, S., Tong, S., Wang, Q., Wang, W., Wang, X., Wang, X., Wang, Z., Wei, L., Whalley, L., Wu, X., Wu, Z., Xie, P., Yang, F., Zhang, Q., Zhang, Y., Zhang, Y., and Zheng, M.: Introduction to the special issue “In-depth study of air pollution sources and processes within Beijing and its surrounding region (APHH-Beijing)”, Atmospheric Chemistry and Physics, 19, 7519-7546, 10.5194/acp-19-7519-2019, 2019.

Shou, Y., Huang, Y., Zhu, X., Liu, C., Hu, Y., and Wang, H.: A review of the possible associations between ambient PM2.5 exposures and the development of Alzheimer's disease, Ecotoxicol Environ Saf, 174, 344-352, 10.1016/j.ecoenv.2019.02.086, 2019.

Sorensen, C.M., 2001. Light Scattering by Fractal Aggregates: A Review. Aerosol Science and Technology, 35(2): 648-687.

Sun, Y., Zhuang, G., Tang, A., Wang, Y., and An, Z.: Chemical Characteristics of PM2.5 and PM10 in Haze−Fog Episodes in Beijing, Environmental Science & Technology, 40, 3148-3155, 10.1021/es051533g, 2006.

Sun, Y., Jiang, Q., Wang, Z., Fu, P., Li, J., Yang, T., and Yin, Y.: Investigation of the sources and evolution processes of severe haze pollution in Beijing in January 2013, Journal of Geophysical Research: Atmospheres, 119, 4380-4398, 10.1002/2014jd021641, 2014.

Sun, Y., Du, W., Wang, Q., Zhang, Q., Chen, C., Chen, Y., Chen, Z., Fu, P., Wang, Z., Gao, Z., and Worsnop, D. R.: Real-Time Characterization of Aerosol Particle Composition above the Urban Canopy in Beijing: Insights into the Interactions between the Atmospheric Boundary Layer and Aerosol Chemistry, Environ Sci Technol, 49, 11340-11347, 10.1021/acs.est.5b02373, 2015.

Sun, Y., Du, W., Fu, P., Wang, Q., Li, J., Ge, X., Zhang, Q., Zhu, C., Ren, L., Xu, W., Zhao, J., Han, T., Worsnop, D. R., and Wang, Z.: Primary and secondary aerosols in Beijing in winter: sources, variations and

processes, Atmospheric Chemistry and Physics, 16, 8309-8329, 10.5194/acp-16-8309-2016, 2016.

Sun, Y. L., Wang, Z. F., Fu, P. Q., Yang, T., Jiang, Q., Dong, H. B., Li, J., and Jia, J. J.: Aerosol composition, sources and processes during wintertime in Beijing, China, Atmospheric Chemistry and Physics, 13, 4577-4592, 10.5194/acp-13-4577-2013, 2013.

Tang, M., Cziczo, D. J., and Grassian, V. H.: Interactions of Water with Mineral Dust Aerosol: Water Adsorption, Hygroscopicity, Cloud Condensation, and Ice Nucleation, Chem Rev, 116, 4205-4259, 10.1021/acs.chemrev.5b00529, 2016.

Tao, J., Zhang, L., Cao, J., and Zhang, R.: A review of current knowledge concerning PM_{2. 5} chemical composition, aerosol optical properties and their relationships across China, Atmospheric Chemistry and Physics, 17, 9485-9518, 10.5194/acp-17-9485-2017, 2017.

562 Unga, F., Choël, M., Derimian, Y., Deboudt, K., Dubovik, O., and Goloub, P.: Microscopic Observations of
563 Core-Shell Particle Structure and Implications for Atmospheric Aerosol Remote Sensing, Journal of
564 Geophysical Research: Atmospheres, 123, 13,944-913,962, 10.1029/2018jd028602, 2018.

565 Wang, G., Zhang, R., Gomez, M. E., Yang, L., Levy Zamora, M., Hu, M., Lin, Y., Peng, J., Guo, S., Meng, J.,
566 Li, J., Cheng, C., Hu, T., Ren, Y., Wang, Y., Gao, J., Cao, J., An, Z., Zhou, W., Li, G., Wang, J., Tian, P., Marrero-
567 Ortiz, W., Secrest, J., Du, Z., Zheng, J., Shang, D., Zeng, L., Shao, M., Wang, W., Huang, Y., Wang, Y., Zhu,
568 Y., Li, Y., Hu, J., Pan, B., Cai, L., Cheng, Y., Ji, Y., Zhang, F., Rosenfeld, D., Liss, P. S., Duce, R. A., Kolb, C. E.,
569 and Molina, M. J.: Persistent sulfate formation from London Fog to Chinese haze, Proc Natl Acad Sci U S
570 A, 113, 13630-13635, 10.1073/pnas.1616540113, 2016.

571 Wang, Q., Sun, Y., Xu, W., Du, W., Zhou, L., Tang, G., Chen, C., Cheng, X., Zhao, X., Ji, D., Han, T., Wang,
572 Z., Li, J., and Wang, Z.: Vertically resolved characteristics of air pollution during two severe winter haze
573 episodes in urban Beijing, China, Atmospheric Chemistry and Physics, 18, 2495-2509, 10.5194/acp-18-
574 2495-2018, 2018.

575 Wang, W., Shao, L., Guo, M., Hou, C., Xing, J., and Wu, F.: Physicochemical Properties of Individual
576 Airborne Particles in Beijing during Pollution Periods, Aerosol and Air Quality Research, 17, 3209-3219,
577 10.4209/aaqr.2017.03.0116, 2017.

578 Wang, X., Cotter, E., Iyer, K. N., Fang, J., Williams, B. J., and Biswas, P.: Relationship between pyrolysis
579 products and organic aerosols formed during coal combustion, Proceedings of the Combustion Institute,
580 35, 2347-2354, 10.1016/j.proci.2014.07.073, 2015.

581 Wang, Y., Yao, L., Wang, L., Liu, Z., Ji, D., Tang, G., Zhang, J., Sun, Y., Hu, B., and Xin, J.: Mechanism for the
582 formation of the January 2013 heavy haze pollution episode over central and eastern China, Science
583 China Earth Sciences, 57, 14-25, 10.1007/s11430-013-4773-4, 2013.

584 Wehner, B., Siebert, H., Ansmann, A., Ditas, F., Seifert, P., Stratmann, F., Wiedensohler, A., Apituley, A.,
585 Shaw, R. A., Manninen, H. E., and Kulmala, M.: Observations of turbulence-induced new particle
586 formation in the residual layer, Atmospheric Chemistry and Physics, 10, 4319-4330, 10.5194/acp-10-
587 4319-2010, 2010.

588 Li, W., Xu, L., Liu, X., Zhang, J., Lin, Y., Yao, X., Gao, H., Zhang, D., Chen, J., Wang, W., Harrison, R. M.,
589 Zhang, X., Shao, L., Fu, P.: Athanasios Nenes, and Zongbo Shi: Air pollution–aerosol interactions produce
590 more bioavailable iron for ocean ecosystems, Science Advance, 3, e1601749, 2017.

591 Xia, Y., Guan, D., Meng, J., Li, Y., and Shan, Y.: Assessment of the pollution–health–economics nexus in
592 China, Atmospheric Chemistry and Physics, 18, 14433-14443, 10.5194/acp-18-14433-2018, 2018.

593 Xu, L., Liu, L., Zhang, J., Zhang, Y., Ren, Y., Wang, X., and Li, W.: Morphology, Composition, and Mixing
594 State of Individual Aerosol Particles in Northeast China during Wintertime, Atmosphere, 8,
595 10.3390/atmos8030047, 2017.

596 Xu, L., Zhang, D., and Li, W.: Microscopic comparison of aerosol particles collected at an urban site in
597 North China and a coastal site in Japan, Sci Total Environ, 669, 948-954, 10.1016/j.scitotenv.2019.03.163,
598 2019.

599 Yuan, Q., Li, W., Zhou, S., Yang, L., Chi, J., Sui, X., and Wang, W.: Integrated evaluation of aerosols during
600 haze-fog episodes at one regional background site in North China Plain, Atmospheric Research, 156,

102-110, 10.1016/j.atmosres.2015.01.002, 2015.

Zhang, D., Chen, B., Yamada, M., Niu, H., Wang, B., Iwasaka, Y., and Shi, G.: Elevated soot layer in polluted atmosphere: A case study in Beijing, Journal of the Meteorological Society of Japan., 90, 361-375, 10.2151/jmsj.2012-302, 2012.

Zhang, J., Liu, L., Wang, Y., Ren, Y., Wang, X., Shi, Z., Zhang, D., Che, H., Zhao, H., Liu, Y., Niu, H., Chen, J., Zhang, X., Lingaswamy, A. P., Wang, Z., and Li, W.: Chemical composition, source, and process of urban aerosols during winter haze formation in Northeast China, Environ Pollut, 231, 357-366, 10.1016/j.envpol.2017.07.102, 2017.

Zhang, J., Liu, L., Xu, L., Lin, Q., Zhao, H., Wang, Z., Guo, S., Hu, M., Liu, D., Shi, Z., Huang, D., and Li, W.: Exploring wintertime regional haze in northeast China: role of coal and biomass burning, Atmos. Chem. Phys., 20, 5355-5372, 10.5194/acp-20-5355-2020, 2020.

Zhang, Q., Ma, X., Tie, X., Huang, M., and Zhao, C.: Vertical distributions of aerosols under different weather conditions: Analysis of in-situ aircraft measurements in Beijing, China, Atmospheric Environment, 43, 5526-5535, https://doi.org/10.1016/j.atmosenv.2009.05.037, 2009.

Zhou, W., Sun, Y., Xu, W., Zhao, X., Wang, Q., Tang, G., Zhou, L., Chen, C., Du, W., Zhao, J., Xie, C., Fu, P., and Wang, Z.: Vertical Characterization of Aerosol Particle Composition in Beijing, China: Insights From 3 - Month Measurements With Two Aerosol Mass Spectrometers, Journal of Geophysical Research: Atmospheres, 123, 13,016-013,029, 10.1029/2018jd029337, 2018a.

Zhou, W., Wang, Q., Zhao, X., Xu, W., Chen, C., Du, W., Zhao, J., Canonaco, F., Prévôt, A. S. H., Fu, P., Wang, Z., Worsnop, D. R., and Sun, Y.: Characterization and source apportionment of organic aerosol at 260 m on a meteorological tower in Beijing, China, Atmospheric Chemistry and Physics, 18, 3951-3968, 10.5194/acp-18-3951-2018, 2018b.

Zhu, J., Crozier, P. A., and Anderson, J. R.: Characterization of light-absorbing carbon particles at three altitudes in East Asian outflow by transmission electron microscopy, Atmospheric Chemistry and Physics, 13, 6359-6371, 10.5194/acp-13-6359-2013, 2013.

627 Table 1 Sample information and meteorological conditions

Sample ID①	Date (2016)	Time ②	$PM_{2.5}$ ($\mu g\ m^{-3}$)	SO_2 ($\mu g\ m^{-3}$)	NO_2 ($\mu g\ m^{-3}$)	O_3 ($\mu g\ m^{-3}$)	RH (%)	T (℃)	MLH (m)③
Z1-1	12/1	9:10	12④	2	48	37	24	6	--
Z2-1	12/1	8:40	--	--	--	--	--	--	194
Z1-2	12/2	1:00	110	25	109	3	55	2	--
Z2-2	12/2	1:00	--	--	--	--	--	--	141
Z1-3	12/2	9:10	24	20	134	2	50	3	--
Z2-3	12/2	8:40	--	--	--	--	--	--	134
Z1-4	12/3	1:53	142	36	102	6	79	-1	--
Z2-4	12/3	3:00	--	--	--	--	--	--	232
Z1-5	12/4	1:04	530	14	180	4	93	1	--
Z2-5	12/4	3:00	--	--	--	--	--	--	136
Z1-6	12/5	2:00	86	8	21	53	75	2	--
Z2-6	12/5	2:00	--	--	--	--	--	--	114
Z1-7	12/8	9:10	187	2	16	72	86	2	--
Z2-7	12/8	8:40	--	--	--	--	--	--	191
Z1-8	12/9	9:20	12	8	67	12	33	2	--
Z2-8	12/9	8:30	--	--	--	--	--	--	250

628 ①Samples are collected at two altitudes: Z1 is 2 m above ground and Z2 is 280 m above ground.
629 ② Sampling duration ranges from 30 seconds to less than 5 minutes depending on the PM pollution.
630 ③ MLH represents the mixed layer height and the data are 15minutes average; MLH is less than
631 280 m and the samples collected at Z2 represent samples above the mixed layer. ④ If $PM_{2.5}$ mass
632 concentration is less than 75 $\mu g\ m^{-3}$, samples are classified as non-haze samples and if $PM_{2.5}$ mass
633 concentration is more than 75 $\mu g\ m^{-3}$, samples are classified as haze samples.
634

635 Table 2 Classification and characteristics of individual particle types.

Particle type	Elemental composition	Morphology	Possible sources
Soot particles	C and minor amounts of O, Si.	Chain-like or compact C-dominated aggregates.	Incomplete combustion of biomass and fossil fuel.
Organic particles	C and O with minor amounts of Si, K, S, Cl.	Spherical, near spherical or irregular shapes.	Mainly from Combustion process of biomass and fossil fuels.
Mineral particles	O, Si, Al, Ca, Fe, Na, K, Mg, Ti, and S.	Irregular shapes.	Re-suspended from soil dust, road dust, and construction dust.
Metal particles	Fe, Zn, Mn, Ti, and Pb.	Spherical or irregular shapes.	Industries, coal-fired power plants and oil refineries.
S-rich particles	S and O with minor amounts of N, K.	Spherical, near spherical or irregular shapes.	Secondary aerosol formation.
Organic mixed with Sulfur-rich particles	C, O, and S with minor amounts of N, K or Cl.	Irregular shapes.	Secondary aerosol reaction.
Other mixed particles	Complex elemental composition.	Irregular shapes with different particle types.	Secondary aerosol reaction.

636

637 Table 3 Relative number percentage of individual particles.

Air qualities	Sample ID	Number	Metals	Minerals	OPs	S-rich	Soot	OP-S	Other
Non-haze periods	Z1-1	114	2.6	30.7	19.3	36.0	5.3	1.8	4.4
	Z2-1	113	1.8	12.4	16.8	56.6	10.6	0.9	0.9
	Z1-3	135	4.4	34.1	31.9	12.6	11.1	0.7	5.2
	Z2-3	118	2.5	23.7	45.8	17.0	4.2	2.5	4.2
	Z1-8	140	1.4	62.9	12.1	11.4	2.9	2.1	7.1
	Z2-8	119	3.4	33.6	19.3	18.5	17.7	0.0	7.6
	Ave (Z1)	389	2.8	42.5	21.1	20.0	6.4	1.6	5.6
	Ave (Z2)	350	2.6	23.2	27.3	30.7	10.8	1.1	4.2
Haze periods	Z1-2	123	2.4	21.1	42.3	17.1	7.3	2.4	7.3
	Z2-2	164	4.9	14.6	37.2	25.0	4.3	9.8	4.3
	Z1-4	160	0.6	28.8	30.6	8.8	13.8	9.4	8.1
	Z2-4	266	0.0	3.8	53.0	3.4	7.1	19.6	13.2
	Z1-5	461	0.9	6.5	18.9	22.1	7.6	31.5	12.6
	Z2-5	266	0.4	0.4	32.3	7.1	2.3	44.0	13.5
	Z1-6	237	2.5	11.0	21.5	48.5	2.1	6.8	7.6
	Z2-6	281	1.8	11.0	18.9	19.6	12.8	15.3	20.6
	Z1-7	168	1.8	23.2	28.0	20.8	2.4	15.5	8.3
	Z2-7	192	1.6	17.7	32.3	27.1	1.6	15.1	4.7
	Ave (Z1)	1149	1.7	18.1	28.3	23.5	6.6	13.1	8.8
	Ave (Z2)	1169	1.7	9.5	34.7	16.4	5.6	20.7	11.3

638

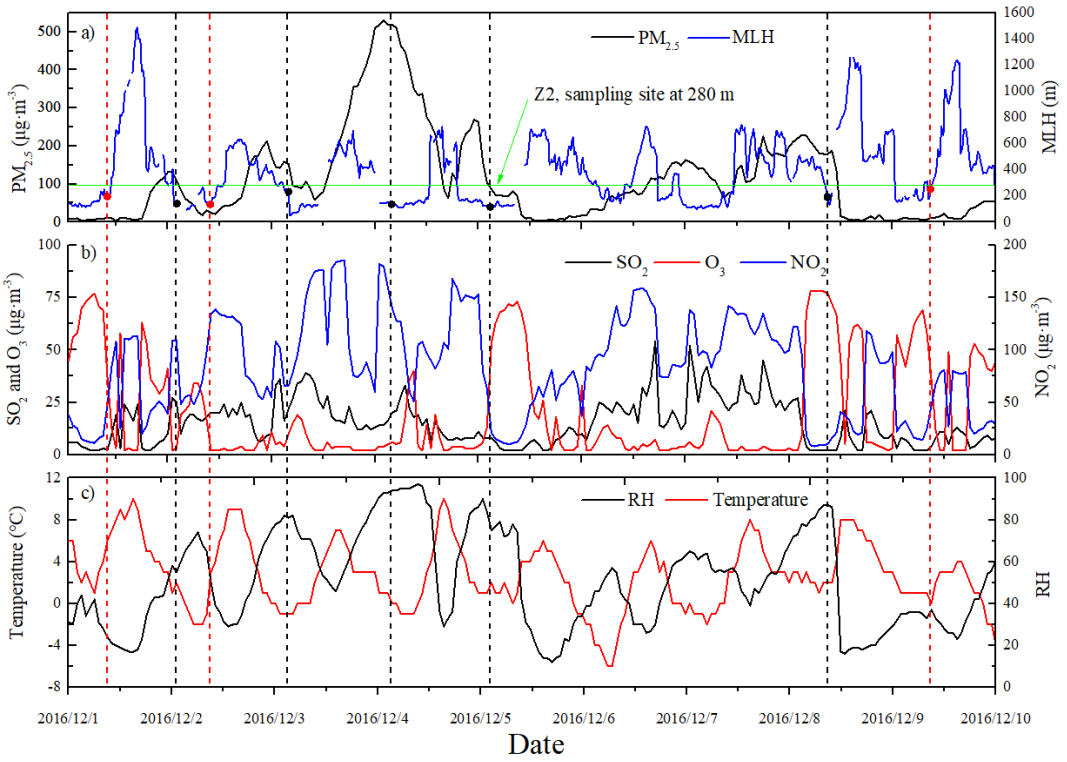

Fig. 1: The dashed lines represent the individual particle sampling times with red lines representing non-haze samples and black lines haze samples. (a) Temporal variations of mixed layer height (MLH) and $PM_{2.5}$ mass concentrations. The solid dots represent the MLH during the sampling times. (b) Temporal variations of SO_2, NO_2, O_3 at ground level at the Olympic Park monitor site, which is the closest national air quality monitor station to the sampling site (~1.5 km). (c) Temporal variations of temperature (T) and relative humidity (RH) at ground level. Date was obtained from the Ministry of Ecology and Environment of China (https://www.aqistudy.cn).

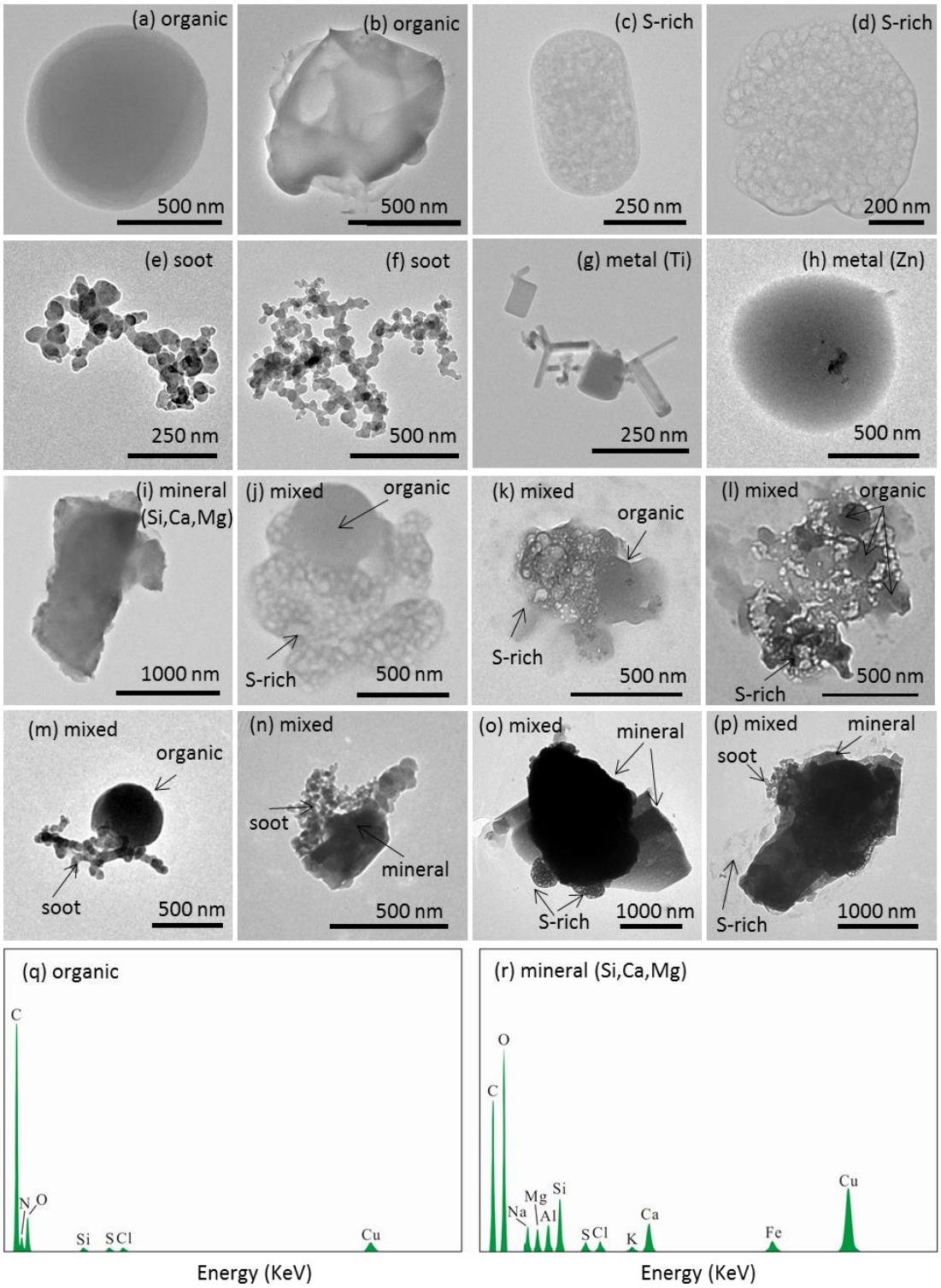

Fig. 2: Examples of morphologies and mixing characteristics of individual aerosol particles in winter in Beijing at ground level and above the mixed layer. (a) Spherical organic particle, (b) irregular shaped organic particle, (c-d) S-rich particles, (e-f) soot particles, (g-h) metal particles, (i) mineral particles, (j-l) OP-S mixed particles, and (m-p) other mixed particle types. (q) and (r) are EDS of (b) and (i). The difference between the particles in (b) and (i) is that organic particles (b) mainly composed C and O while minerals (i) mainly composed O, Si, Ca and Mg.

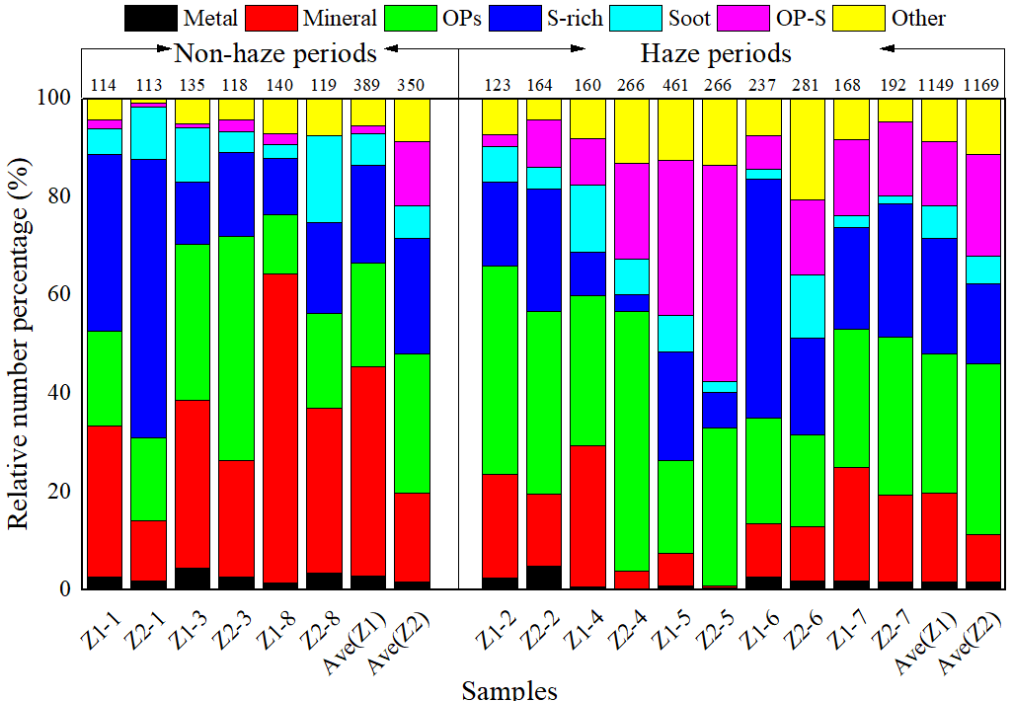

Fig. 3: Relative number percentage of different particle types at ground level (Z1) and above the mixed layer height (Z2). The number above each bar represents the total particle number analyzed in each sample.

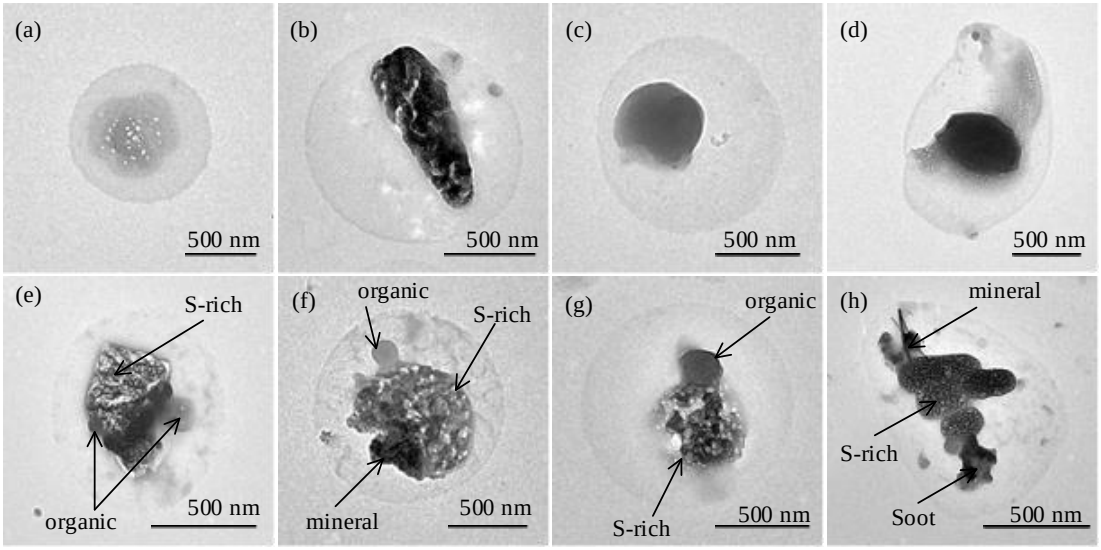

Fig. 4: Images of core-shell structured particles. (a-b) S-rich cores, (c-d) organic cores, and (e-h) mixed cores.

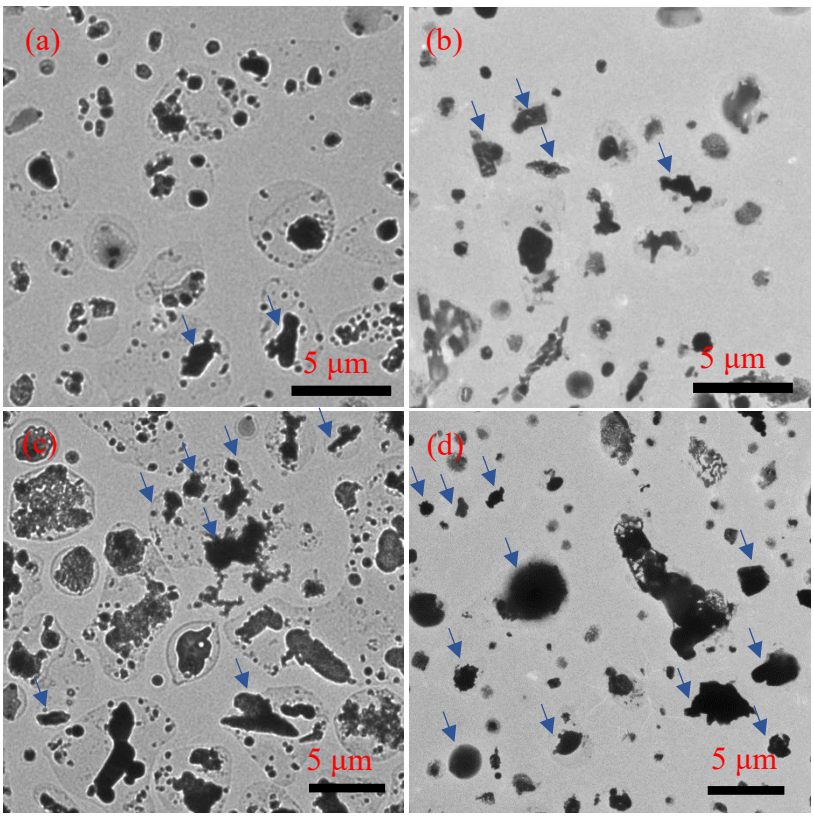

Fig. 5: Low magnification images of individual particles. (a) and (c) are particles above the mixed layer (MLH) at different size ranges. (b) and (d) are particles at ground level at different size ranges. More coated particles were found above the MLH. Arrows show part of the mineral particles.

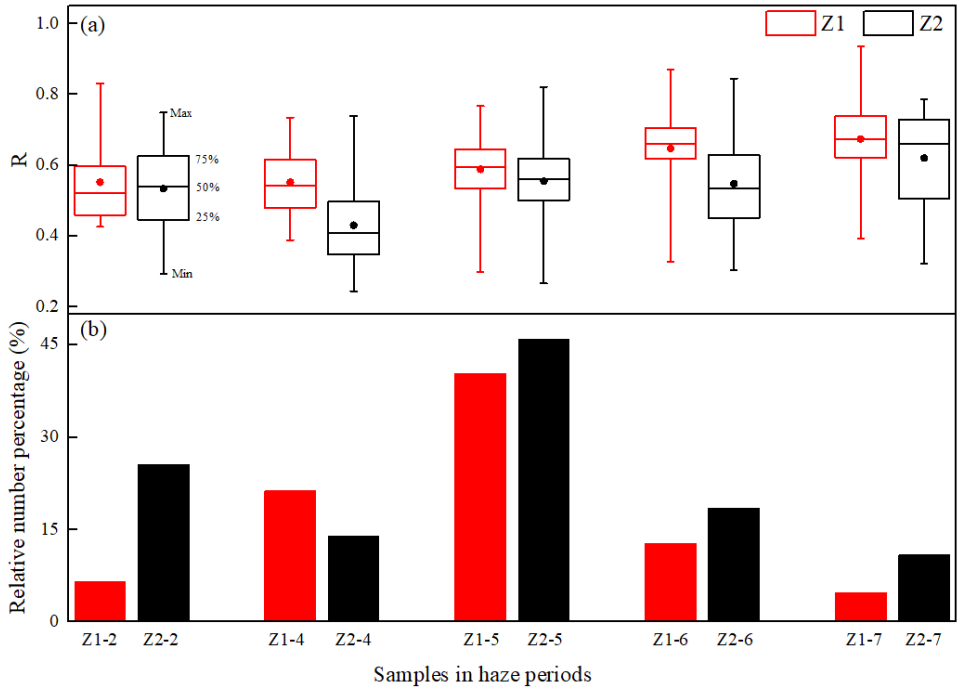

Fig. 6: (a) R is C/S ratio (D_{Aeq} ratio of the core to the whole particle including the shell) of particles during haze periods at ground level (Z1) and above the mixed layer height (Z2); solid dots represent the average value, and (b) the corresponding relative number percentage of core-shell structured particles.

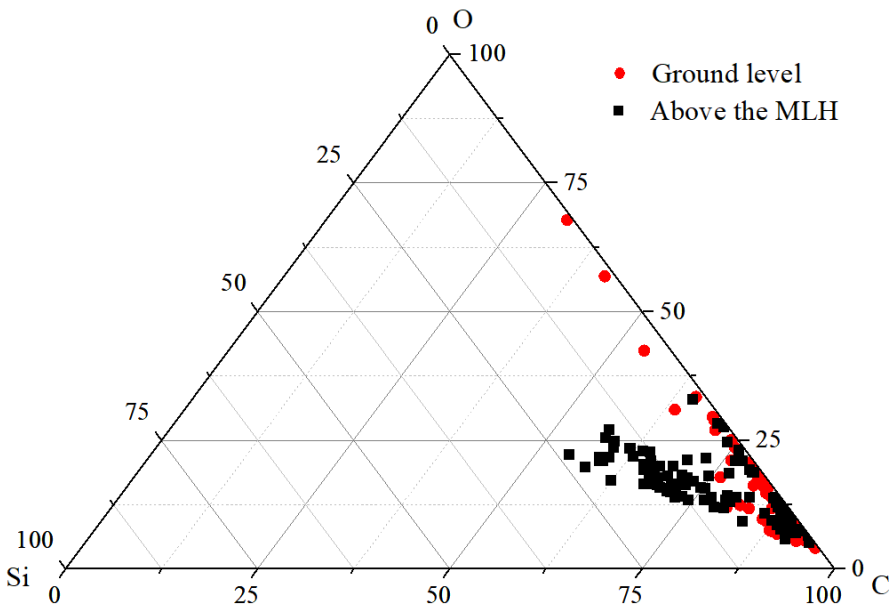

Fig. 7: Triangular diagram showing the weight ratio of C-O-Si of organic particles (OP) at ground level and above the mixed layer height (MLH).